JOURNAL OF SOLID STATE CHEMISTRY 88, 303–323 (1990)

Nanostructure Evolution during Chemical Processing of Gels: A High-Resolution Electron Microscope Study. 1. Rare Earth Oxide and Hydroxycarbonate Colloids

Z. C. KANG AND L. EYRING

Department of Chemistry and The Center for Solid State Science, Arizona State University, Tempe, Arizona 85287

Received May 2, 1990

DEDICATED TO J. M. HONIG ON THE OCCASION OF HIS 65TH BIRTHDAY

The steps in the evolution of colloidal gels during drying, aging, and crystallization into ceramic oxides are followed by high-resolution electron microscopy. Two systems are discussed in this paper. Colloidal ceric hydroxide gels in two morphologies were studied. In one, spherical gel particles with only short-range order were observed to dehydrate to polycrystalline CeO_2 with large grain size. In the other a polycrystalline precipitate of CeO_2 was observed to increase its order without altering its grain size. Colloidal terbium hydroxycarbonate is also observed to have short-range order even in the earliest stages. In contrast to the cerium oxide these disordered materials are observed to crystallize and decompose in dynamic stages (even revealing reversibilities) through the intermediate dioxymonocarbonate to the oxide as carbon dioxide and water are removed. Observations are made by real-time video recording and time-lapse photography.

Introduction

The need for alternative and generally lower temperature routes to the synthesis and processing of materials to fill specific requirements has and is being made eloquently almost daily. There is a vast and growing literature in the field of sol–gel chemical processing. For overviews or general discussions see, for example, Ulrich (*1*), Zelinski and Uhlmann (*2*), or Barringer and Bowen (*3*). For a review with 546 references on the sol–gel chemistry of transition metal oxides alone, see Livage *et al.* (*4*). Actual procedures for the preparation of the class of colloidal gels of concern to us here are discussed by Matijević (*5*).

The sol–gel routes to lanthanide oxide production via dispersed colloidal particles to be followed here is either by the deprotonation of hydrated cations (*6*) or by the controlled release of anions in aqueous solution (*7*). In the deprotonation of hydrated cations, colloidal particles are formed when the conditions of pH and temperature are carefully controlled. Monodispersed particles are obtained when supersaturation is achieved such as to produce a burst of nuclei that is allowed to grow without subsequent nucleation. The process of ceramic production from hydrated cations in solution, through hydrolysis to the formation of precursor complexes, followed by the condensation and polymerization of the colloidal gel which is dried then fired to produce the final ceramic product is sketched in Fig. 1.

0022-4596/90 $3.00

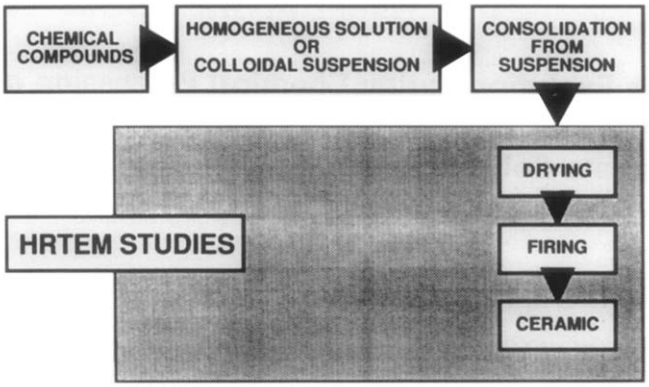

FIG. 1. A flow diagram of the entire chemically derived sol–gel materials process. The part of concern here is outlined.

The chemistry of the early stages of the process is well known and is described in many inorganic chemistry textbooks (*11*). The nature of the precursors and the subsequent steps are known in principle since they have been studied by X-ray, IR, NMR, TEM, and SEM, etc., yet the details are not adequately perceived to satisfy either scientific or technological requirements. The broad aim of these studies is to follow the evolution of the colloidal particles through drying to the crystallization of the product oxide ceramic. High-resolution electron microscopy (HREM) is used for direct observations, near the atomic level, of the texture and structure at each step in the process. The reactions are to be observed both *in situ* and by examination of materials prepared outside the microscope. TGA, DTA, and X-ray studies will aid in the interpretation of the HREM results. An early study of this kind has been reported by Fryer *et al.* (*8*). This paper deals with observations made on freshly precipitated gels using HREM techniques.

Experimental Procedures

The Preparation of Monodispersed Cerium Dioxide Colloids

The cerium-containing colloidal particles were produced (*6*) by hydrolysis initiated by the aging, at elevated temperatures, of solutions containing equal volumes of 1.5 $\times$ 10^{-2} mole dm^{-3} $(NH_4)_2Ce(NO_3)_6$, 6.4 $\times$ 10^{-2} mole dm^{-3} H_2SO_4, and 1.6 $\times$ 10^{-3} mole dm^{-3} Na_2SO_4. The starting solution was at pH 1. Part of the starting solution was aged in an oven at 90°C for 2.5 hr. The cooled solution was at pH 2. Another portion of the original solution was aged at 100°C for 5.6 hr. The carefully washed precipitated gels were suspended in water by sonication and applied to microscope grids supporting holey carbon films.

The Preparation of Terbium Hydroxycarbonate Colloids

The terbium-containing colloid gels were prepared by homogeneous precipitation from warm urea solutions that give controlled release of hydroxyl and carbonate anions (*7*). Equal volumes of 1.4 $\times$ 10^{-2} mole dm^{-3} $TbCl_3$ and 1.7 mole dm^{-3} urea were mixed and aged in an oven at 85°C for 15 hr or at 90°C for 27 hr. The washed aggregated particles were suspended in water using sonication and applied to a microscope grid on which a holey carbon film had been applied.

Electron Microscopy

The specimens supported on holey carbon films were studied in the JEOL 4000EX

a

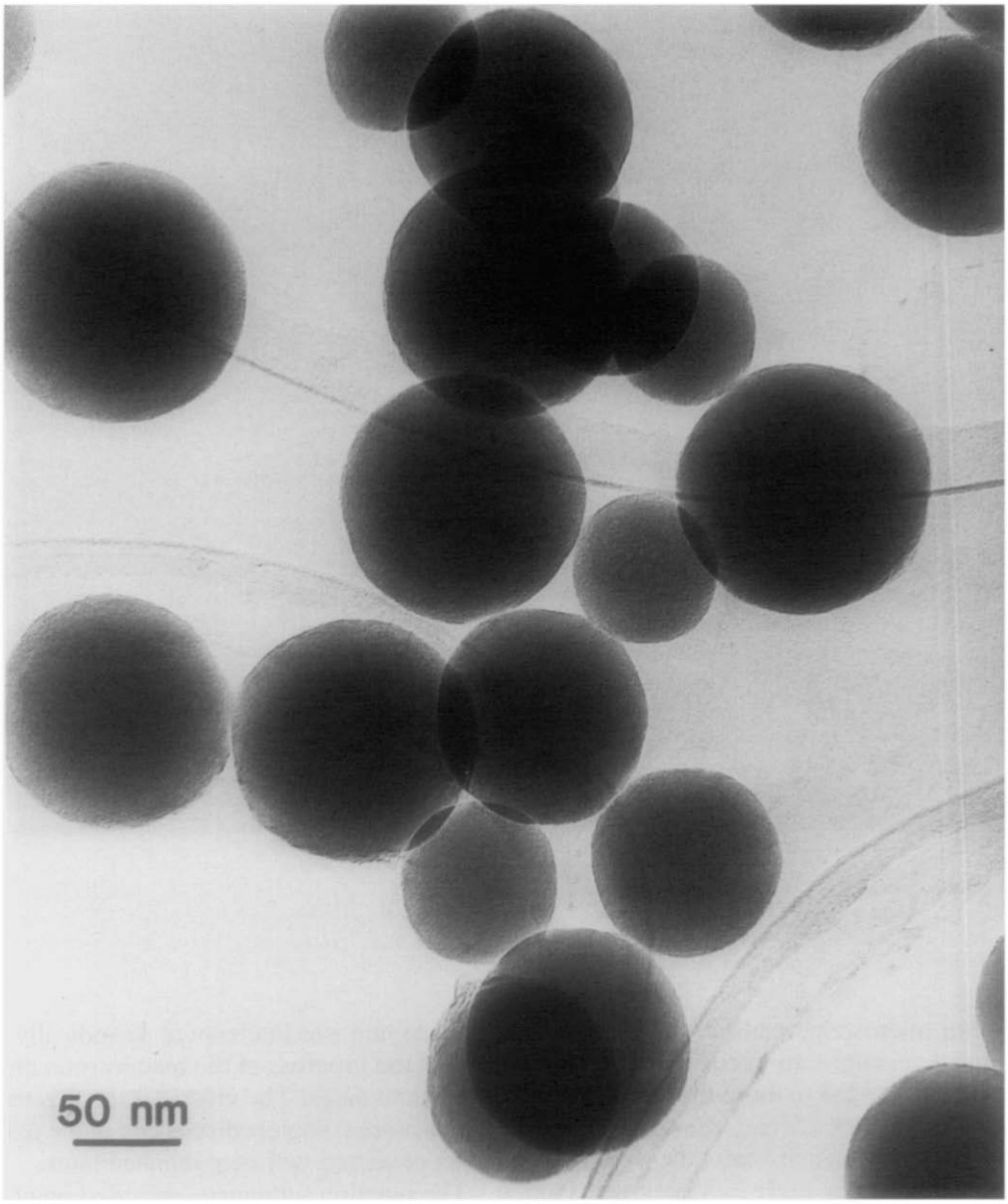

FIG. 2. (a) A high-magnification image of hydrated cerium oxide colloid aged 2.5 hr at 90°C and at an initial pH 1. (b) A high-magnification image of the hydrated cerium oxide colloid formed when the solution was aged at 100°C for 5.6 hr and initial pH 1.

electron microscope at a resolution of about 0.16 nm point-to-point. The top entry microscope was operated at 400 kV at near Scherzer defocus. The beam current was typically 10 A cm^{-2} during imaging and 30 A cm^{-2} during *in situ* irradiation to induce decomposition.

The intense beam and the vacuum of the

b

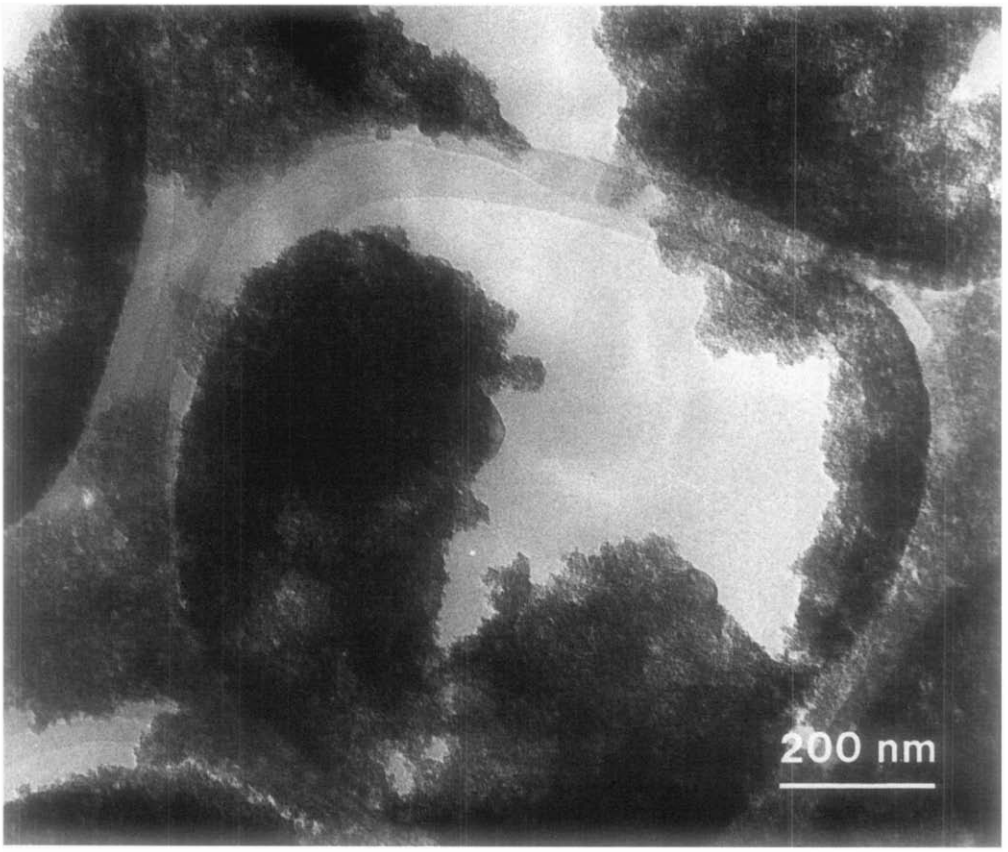

FIG. 2—*Continued*

electron microscope caused a sequence of chemical reactions to occur in the sample that eventually led to more thermally stable products. The 400-kV electrons deposit prodigious energy density into the volume of the material under study by knock-on of the lighter atoms and by a variety of types of radiolysis events. A principal consequence of such irradiation is the elevation of the temperature of the region imaged.

The progress of reactions that propels the gel toward the final oxide product was followed in two ways. Video recordings at 30 frames per second were made during hours of continuous specimen irradiation. The video taping was interrupted periodically to record the progress of the reactions on photographic plates. The video results together with a more complete discussion of the reactions observed will be published later.

The reaction sequences recorded on photographic film were analyzed by careful examination of enlarged prints, but especially by optical diffraction from selected areas of interest. The optical bench system was calibrated by measurement of diffraction patterns from samples of cubic CeO_2 and the perovskite $Pb(Ta_{0.5}Sc_{0.5})O_3$. The lattice parameters obtained in these experiments are believed accurate to within ± 0.02 nm,

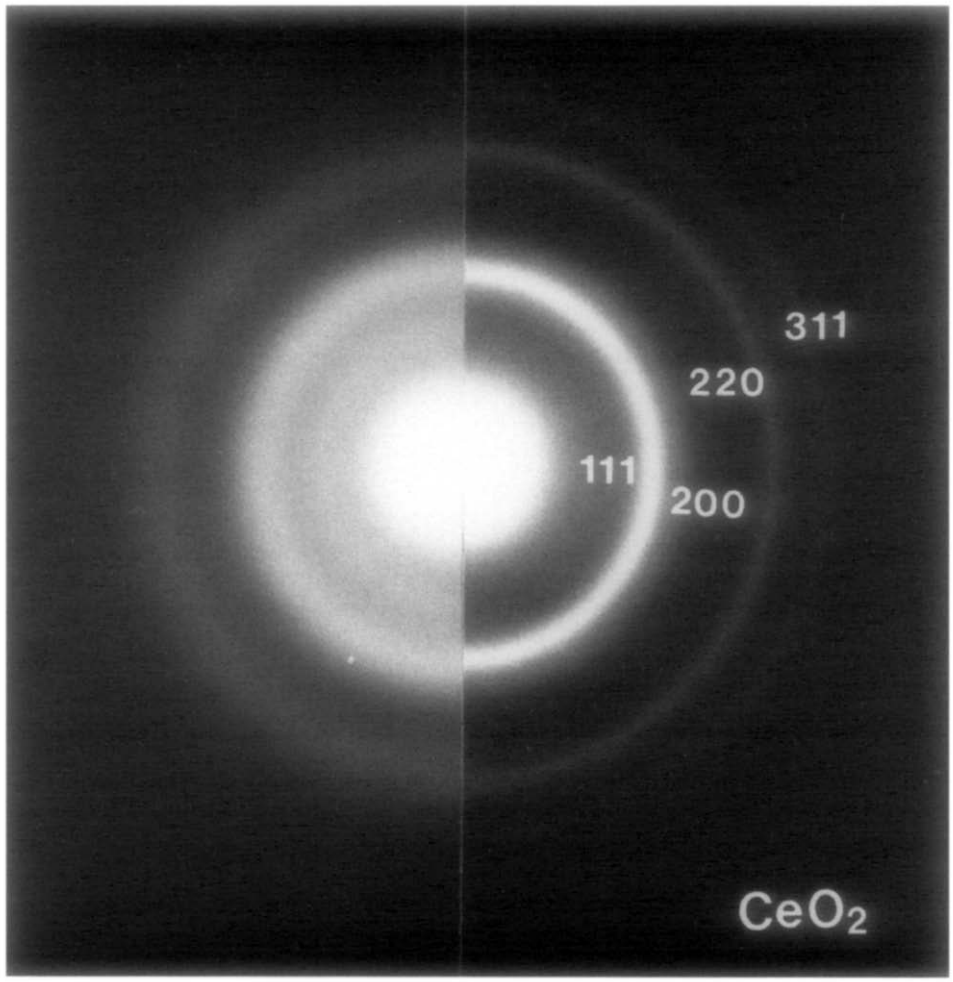

FIG. 3. Juxtaposed diffraction patterns of the specimens shown in Fig. 2. The indexing is based on the fluorite CeO_2.

sufficient in most instances to distinguish between the known decomposition products.

Results and Discussion

The Cerium Dioxide Colloids

A high magnification image of the cerium colloid formed by aging the starting solution (pH 1) at 90°C for 2.5 hr is shown in Fig. 2a. The nearly spherical particles vary from about 140 to about 75 nm in diameter. The particles are already stuck together enough to support each other over the holes in the amorphous carbon film.

The cerium specimen aged at 100°C has undergone a drastic modification (Fig. 2b). It appears that the clusters of particles have aggregated and crystallized in the process yielding a rather coherent mass of very small crystallites.

Early electron diffraction patterns of each of the two samples are shown juxtaposed in

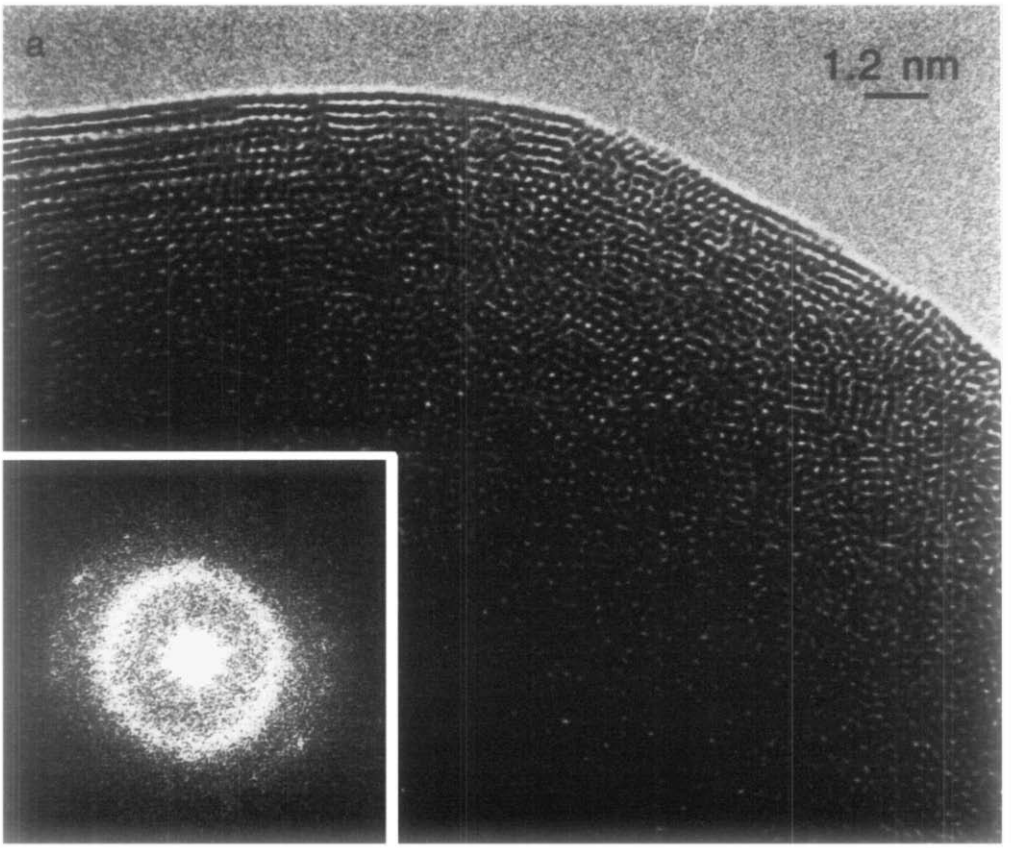

FIG. 4. (a) A high-resolution image of the edge of a sphere from the preparation shown in Fig. 2a. The inset is an optical diffraction pattern. (b) A high-resolution image of the edge of the precipitate shown in Fig. 2b. The inset is an optical diffraction pattern.

Fig. 3. The rings marked (111), (200), (220), and (311) on the right arise from CeO_2 crystallites. Only the first three rings are apparent on the left however there is a weak, broad inner ring only in the pattern from the spherical particles corresponding to a spacing of about 0.45 nm. The rings from the spherical colloid are much more diffuse than those from the crystalline precipitate implying similar but smaller clusters of disordered CeO_2-like structure.

Hsu *et al.* (*6*) report sulfate contamination in their preparations that disappear at temperatures above 200°C. It is believed that the extra inside ring in the left pattern is due to some undecomposed sulfate-containing species. The diffraction patterns correspond well with the high-magnification images of Figs. 2a and 2b and the high-resolution images of Figs. 4a and 4b. Note especially the small areas of more widely spaced layers on the left side of Fig. 4a, believed to be due to sulfate contamination.

It is clear that even the colloidal spheres have substantial order as they are first probed for diffraction in the microscope. This suggests that the polymerized gel possesses a framework having essentially the

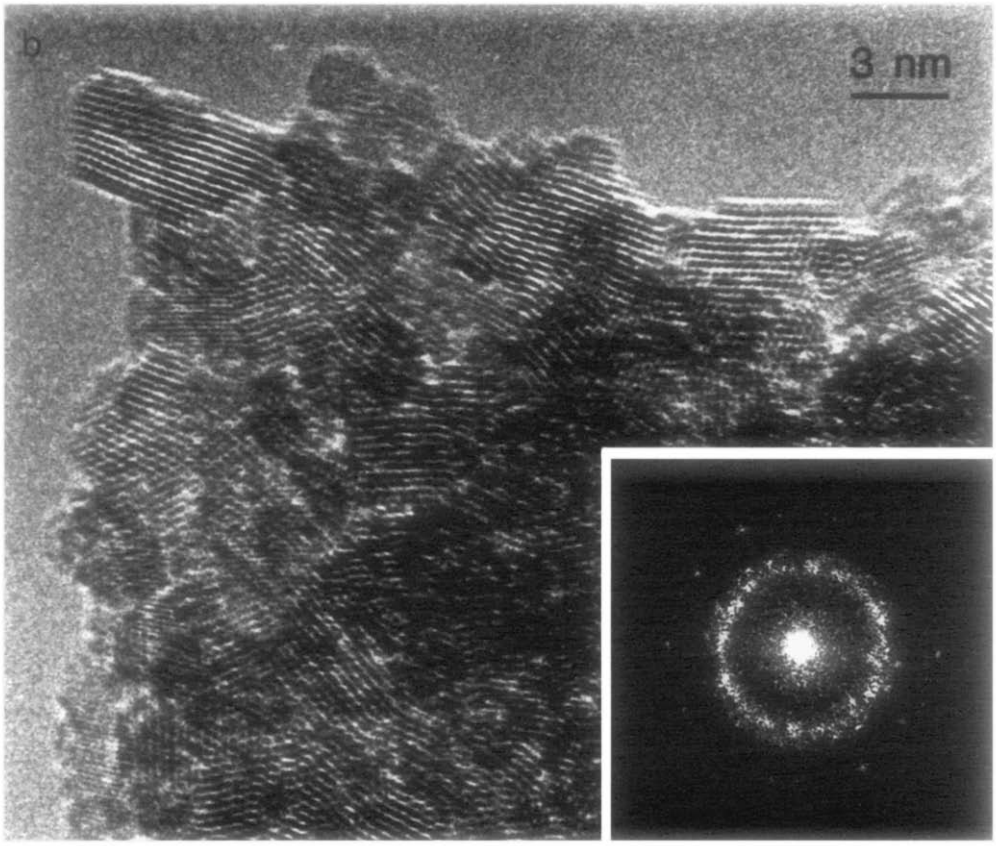

FIG. 4—*Continued*

fluorite arrangement of atoms over small distances. Figure 4a shows a high-resolution image together with an optical diffraction pattern of the edge of one of the colloidal spheres. The broad rings are present, yet some spots are beginning to appear indicating crystal growth induced by the electron beam. The image demonstrates packing of atoms in almost but not quite a regular way at the left-hand side (polygonization of the curved edge has not proceeded very far). The regular, wider spacing at the right could be due to the small content of a complex sulfate responsible for the extra inside ring observed in Fig. 3.

In contrast to the spheres, the crystalline material (Fig. 4b) consists of small and imperfect grains approximately 4 nm across with irregular boundaries. (Notice, for example, the edge dislocation in the grain projecting from the upper left corner.) The rather broad rings of the optical diffraction pattern are spotty as would be expected from such a polycrystalline material.

A characteristic feature of the spheres is that they stick together in clumps. Figures 5a–5d show the progressive sintering of three spheres induced by the electron beam. As sintering proceeds, ordering and crystallization increase as indicated by the apparent polygonization and the appearance of fringes in the later images. The temperature

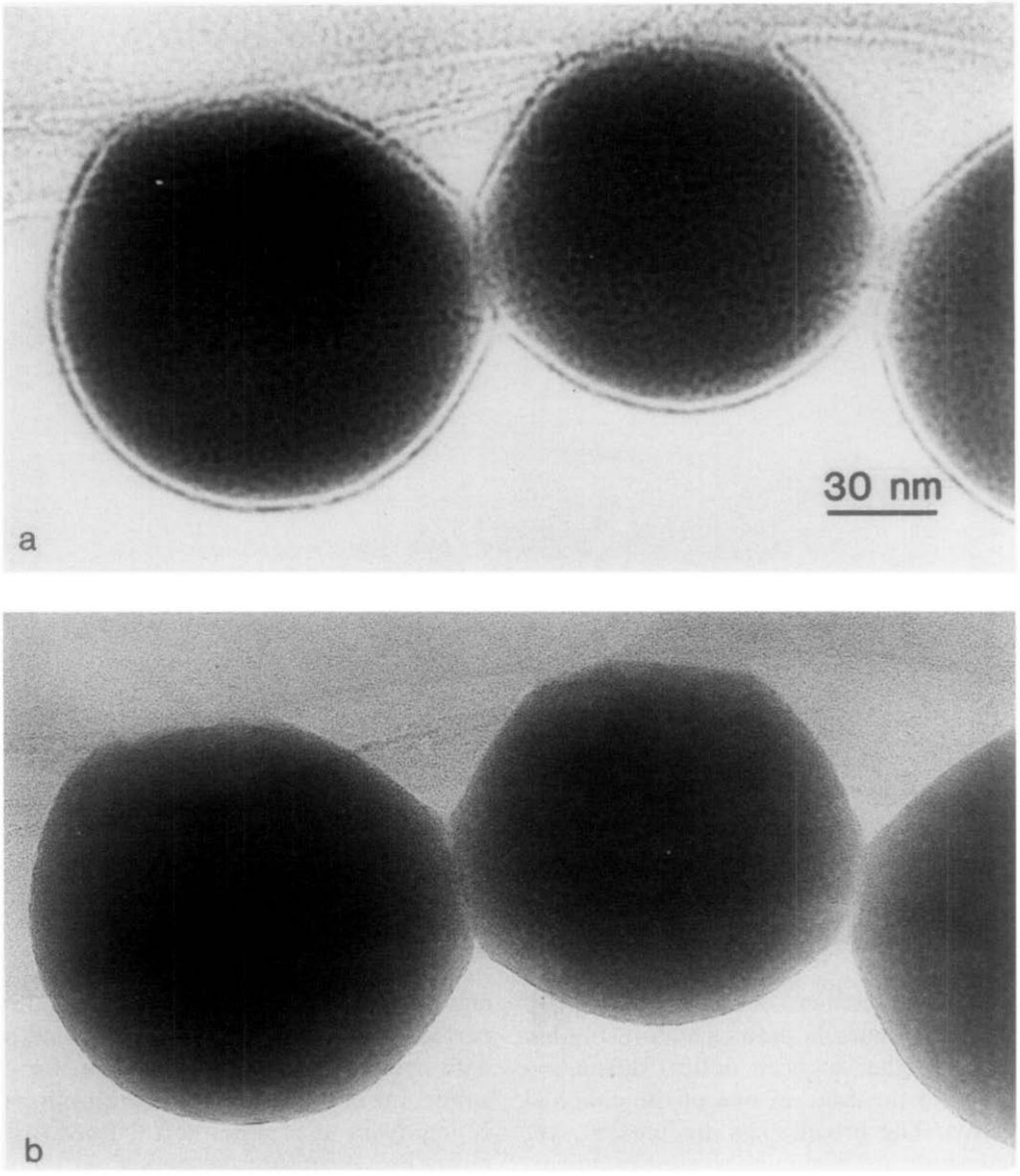

FIG. 5. (a–d) High-magnification images showing the progressive sintering of three spherical particles from the specimen shown in Fig. 2a.

of the spheres is probably less than 200°C. It is of interest to observe the nature of the sintered interface as portrayed at high resolution in Fig. 6. The neck is at the minimum of the crystal profile. The region near the surface does show a disturbed tilt boundary. However, in the deeper regions the boundary is not apparent at all. The occurrence of the boundary in the surface layers is probably because crystallization begins at the surface as solvent is lost to the vacuum and is well advanced when sintering begins. This

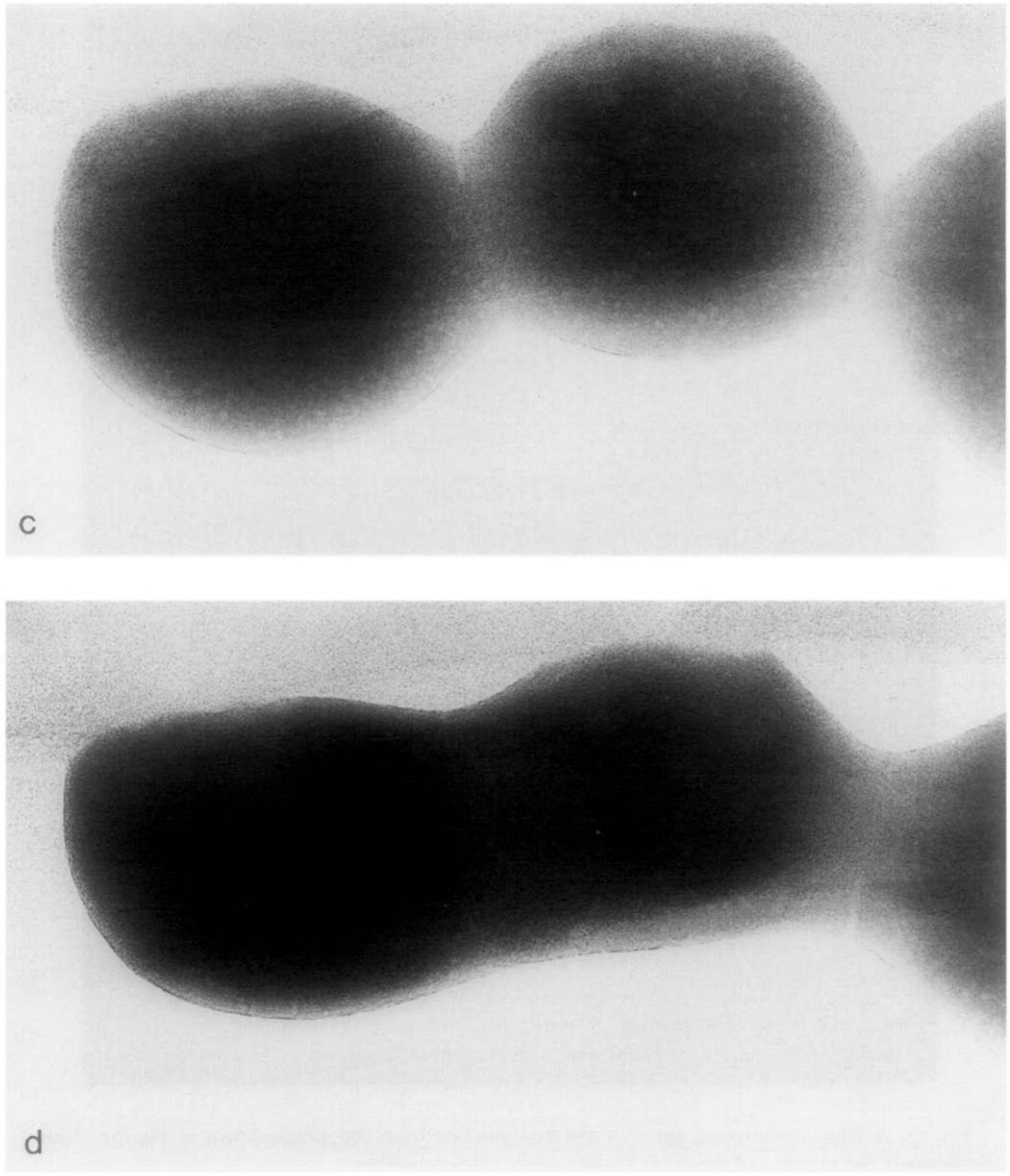

FIG. 5—*Continued*

series of images suggests that if the gelatinous spheres were close packed before sintering begins the product would have a small uniform pore size without sharp grain boundaries. The time interval of radiation to produce the observed sintering sequence is about 15 min.

After beam heating the polycrystalline specimen for the same length of time as needed to obtain Figs. 5 and 6 the high-resolution image shown in Fig. 7 was obtained. It is noteworthy that the grain size does not appear to have changed greatly although the contours at the edge have al-

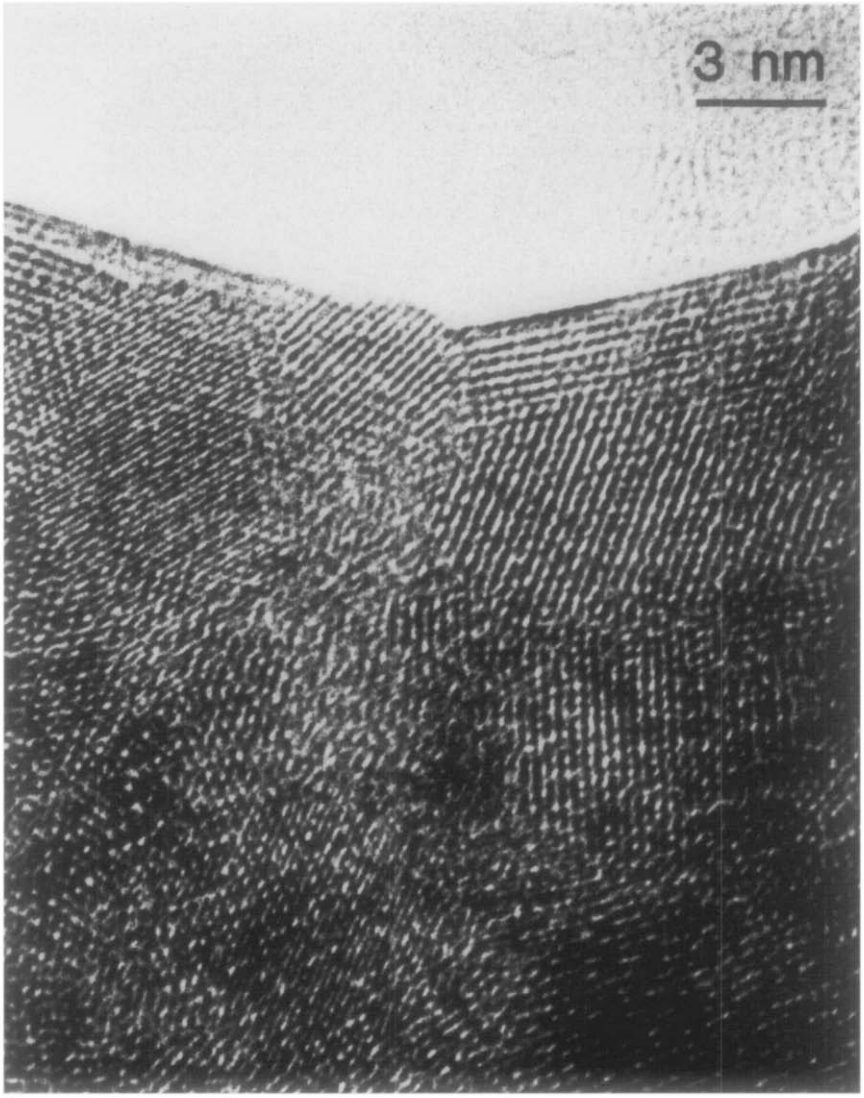

FIG. 6. A high-resolution image of a sintered junction from the group shown in Fig. 5d. Note particularly the absence of a grain boundary in the thicker regions.

tered considerably. Notice, for example, the elimination of the edge dislocation in the protruding crystallite at the upper left corner of the figure (compare Fig. 4b). The optical diffraction patterns show crystals with the [110] and the [100] orientation. The differences between Figs. 6 and 7 emphasize the importance of sample preparation history on the ultrastructure of the product after electron beam heating (and presumably after conventional heat treatment).

The progress of crystallization within the initially disordered spheres is more clearly shown by the images and optical diffraction

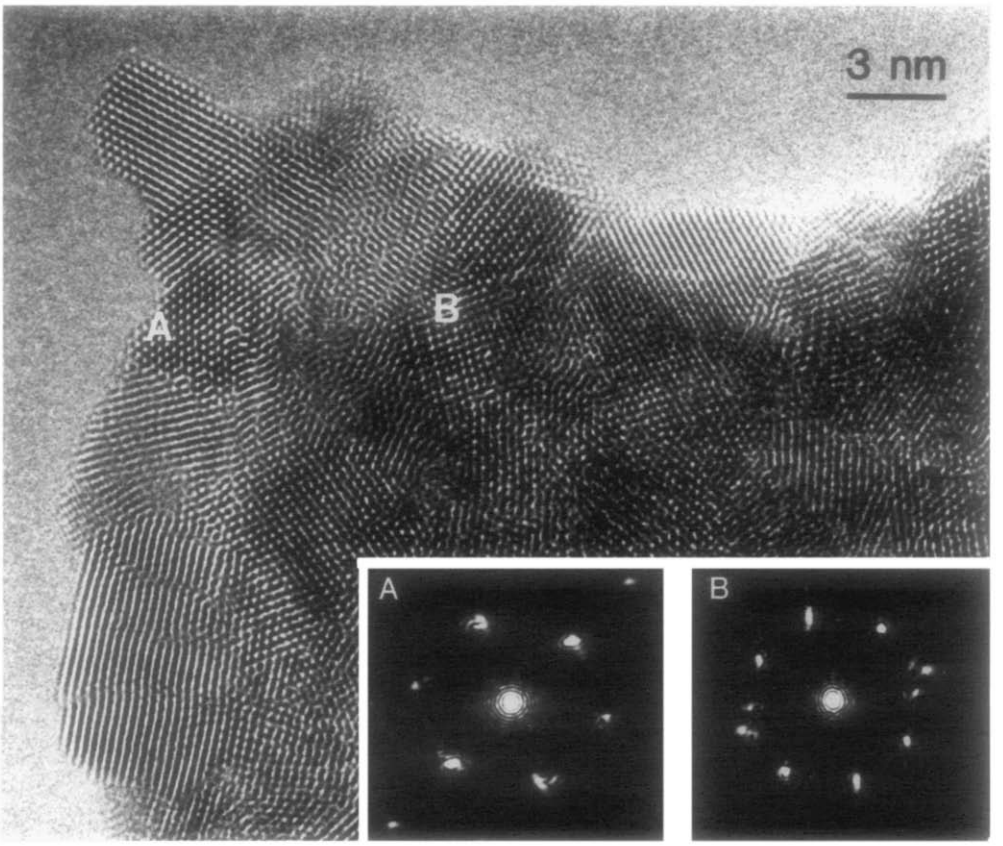

FIG. 7. A high-resolution image of the sample shown in Fig. 3b after about 1 hr irradiation by the electron beam with a flux of 15 A cm^{-2}. Notice the improvement of crystal perfection without significant increase in grain size. The optical diffraction patterns are from the regions marked.

pattern of Fig. 8. Although, the decomposition of the particle is not complete, comparison with Fig. 4a confirms the progress of the reaction. An inner ring of diffraction maxima still reveals the presence of the impurity, assumed to be a sulfate. The strong spots in the pattern are due to a preponderance of crystalline CeO_2 in the [110] orientation. (Observation of the [110] or the [100] orientation of the CeO_2 crystals resulting from electron beam-induced degradation of the colloidal particles is most common). Irradiation by the beam never produced CeO_2 free from impurities even when the beam intensity was 16.5 A cm^{-2}. The apparently more facile crystallization of CeO_2 from the surface inward is consistent with the greater difficulty of the SO_3 molecules to escape from the thicker, central regions of the particles.

The Terbium Hydroxycarbonate Gels

In Fig. 9 the polydisperse specimen obtained when the solution was aged for 12 hr at 85°C is shown in the high-magnification image. The particle sizes fall into two groups; 2 to 3 and 0.5 to 1.5 μm. Clearly,

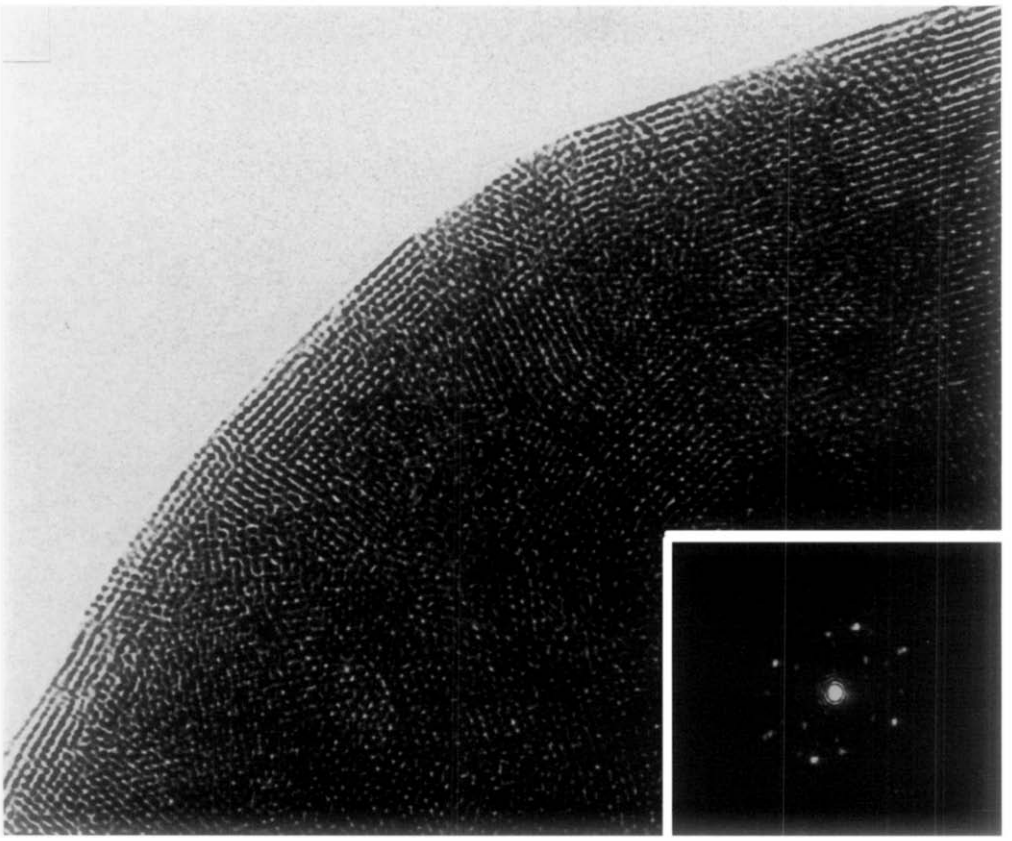

FIG. 8. A high-resolution image of the edge of an aged CeO_x particle together with an optical diffraction pattern of the area marked.

nucleation occurred at different times. The specimen as prepared is grossly clustered with substantial sintering.

The electron diffraction pattern presented in Fig. 10 consists of three broad rings, the outer two of which are centered around spacings of 0.32 and 0.29 nm. These must be characteristic of the inter-metal spacing in the poorly ordered terbium hydroxycarbonate polymer colloid.

The sample aged at 90°C for 27 hr possessed a snowflake-like morphology whose electron diffraction pattern is shown as the left side in Fig. 11. The pattern on the right was taken after 50 min of beam irradiation at 20 A cm^{-2}. Analysis of the patterns reveal that the original specimen was the hydroxycarbonate as expected and that this is decomposed in the electron beam to the Type-II dioxymonocarbonate. A similar pattern of decomposition in the beam is shown when neodymium or praseodymium hydroxycarbonate is decomposed in the electron microscope (*9, 10*). The identification of the decomposition products is by analogy with the corresponding neodymium compounds since there is no previous structural study of the terbium system.

At high-magnification, the effect of the intense beam irradiation on a sphere of the terbium hydroxycarbonate becomes strikingly apparent. Decomposition is accompa-

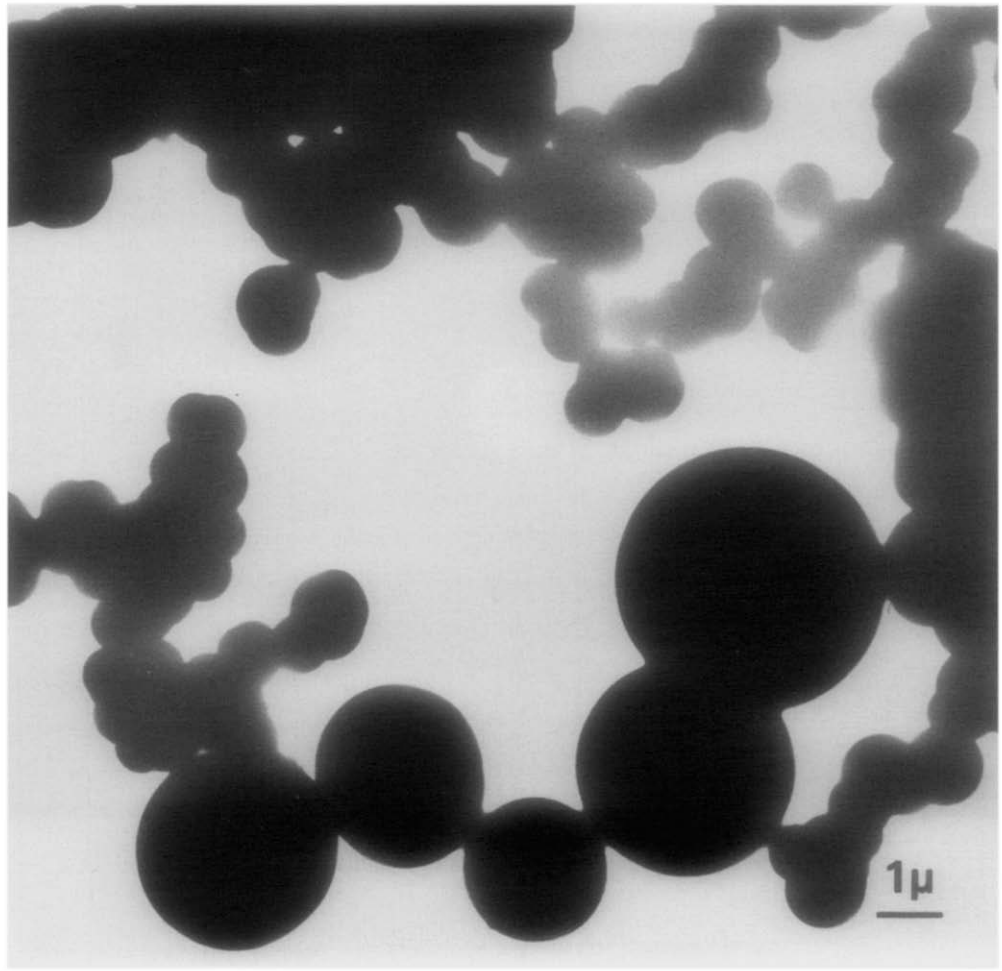

FIG. 9. A polydisperse specimen of $(TbOH)CO_3$ viewed under high-magnification.

nied by marked changes in the contour of the spheres as their volume shrinks by about 25%. Particles sometimes appear to have polygonized during shrinkage; however, they probably have simply become irregular from void formation near the surface. These spheres show large voids, some of which go almost completely through the sphere.

Figure 12 records an image of a sphere of the hydroxycarbonate after substantial decomposition. Compared to earlier images of the particle, the overall volume appears to have been reduced by about 20% during irradiation, and the material of the particle has shifted about dramatically reconstructing the voids accordingly.

A segment of the circumference of the image of Fig. 12 and two antecedents are shown at high-resolution in Figure 13. The central region of these images shows the trnsformation from the hydroxycarbonate through the dioxymonocarbonate to the sesquioxide. The decomposition to the oxide is not complete even in the last image, however.

Figure 14 shows an edge of the snowflake-

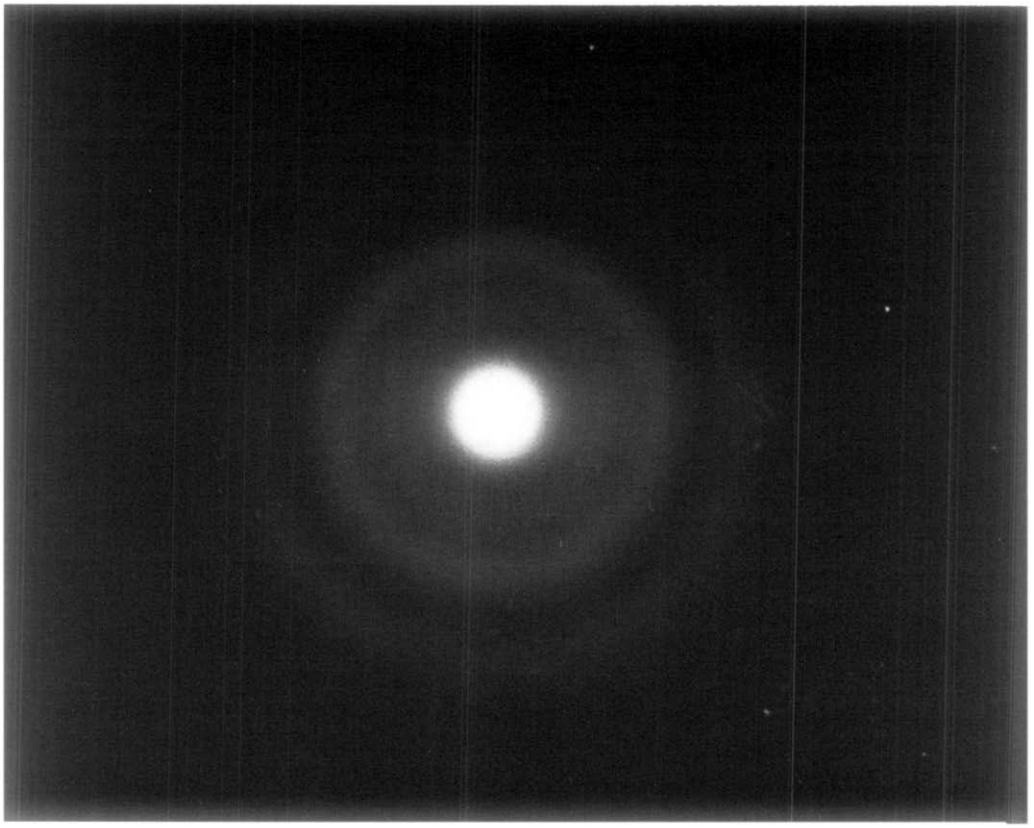

FIG. 10. An electron diffraction pattern of a particle shown in Fig. 8.

like material to be an aggregate of fused spheres consisting of small crystalline domains. This correlates well with the diffraction pattern of Fig. 11. In contrast, the CeO_2 specimen that precipitated in an aggregate of small crystalline domains (Fig. 2b) had distinct grain boundaries. In this aggregate of sintered terbium compounds the crystalline domains can grow and increase in perfection yielding a coarser final product in contrast to the behavior of polycrystalline CeO_2.

Following this survey illustrating the broad features of the $TbOHCO_3$ decomposition just described, an effort was made to observe the earliest stages of reaction. To this end a grid was prepared by dipping it into an unfiltered colloidal suspension. From the individual colloidal particles captured on the carbon film one about 50 nm in diameter was selected for illustration here. During the hours of observation the electron beam was kept at the minimum necessary to record the changes on videotape and by time-lapse photography.

Figure 15a shows a high-magnification image of the 50-nm colloidal particle that was observed as a function of time and is described in the paragraphs that follow. (This particle is from another preparation.) The high-resolution image shown in Fig. 15b, from the area marked in Fig. 15a, was re-

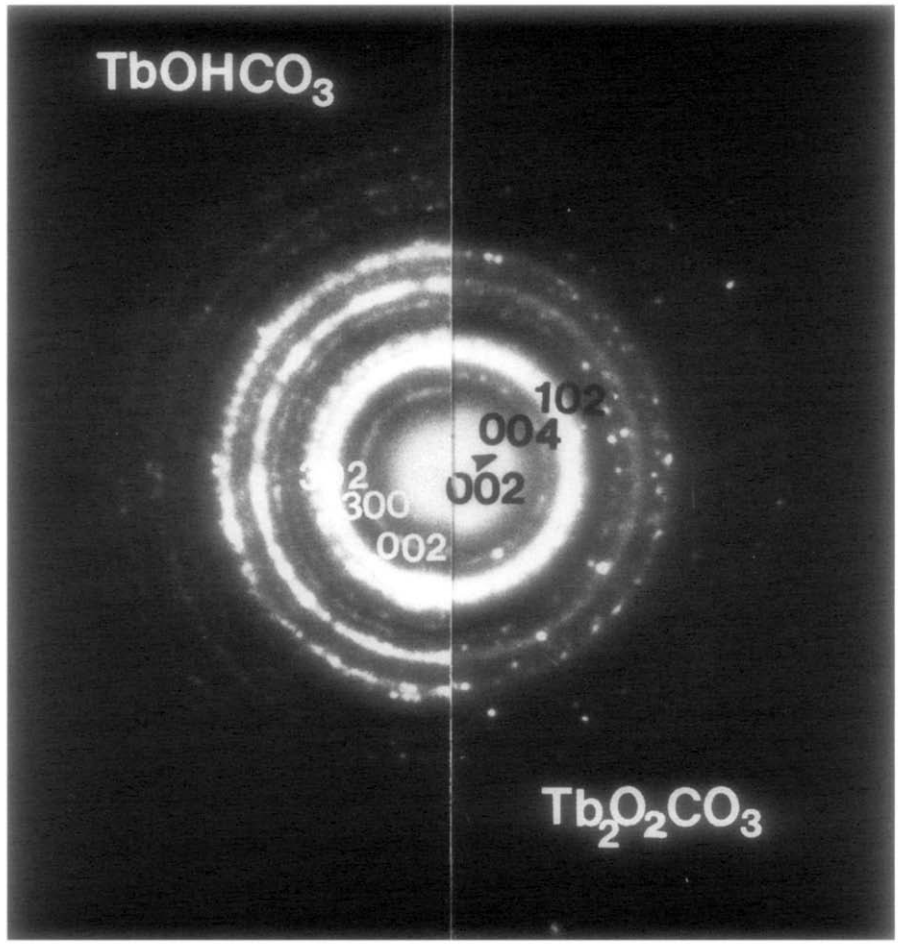

FIG. 11. An electron diffraction pattern of a sample aged at 90°C for 27 hr on the left and on the right the specimen after about 50 min of irradiation. This demonstrates the electron beam decomposition of the hydroxycarbonate.

corded in the first 3 min of observation. A cursory look reveals ordered layers very near the surface as well as some ordered patches further from the edge; however, the degree of order is better displayed by an optical diffraction pattern. The textured ring pattern at the bottom of Fig. 15b was obtained with an aperture of large size. The ring corresponds to small clusters with spacings scattered about 0.31 nm. This is close to the spacing of the (111) planes of the fluorite TbO_2 corresponding to the closest approach of the heavy metal atoms cubicly coordinated by oxygen atoms. The other diffraction patterns are obtained using a very small laser aperture as marked by the adjacent circle on the diagram. The patterns from the small regions of the interior have a preferred orientation with a spacing close to that of cubic close packing of atoms. The atomic rows in certain areas of the surface have a somewhat variable and larger spacing corre-

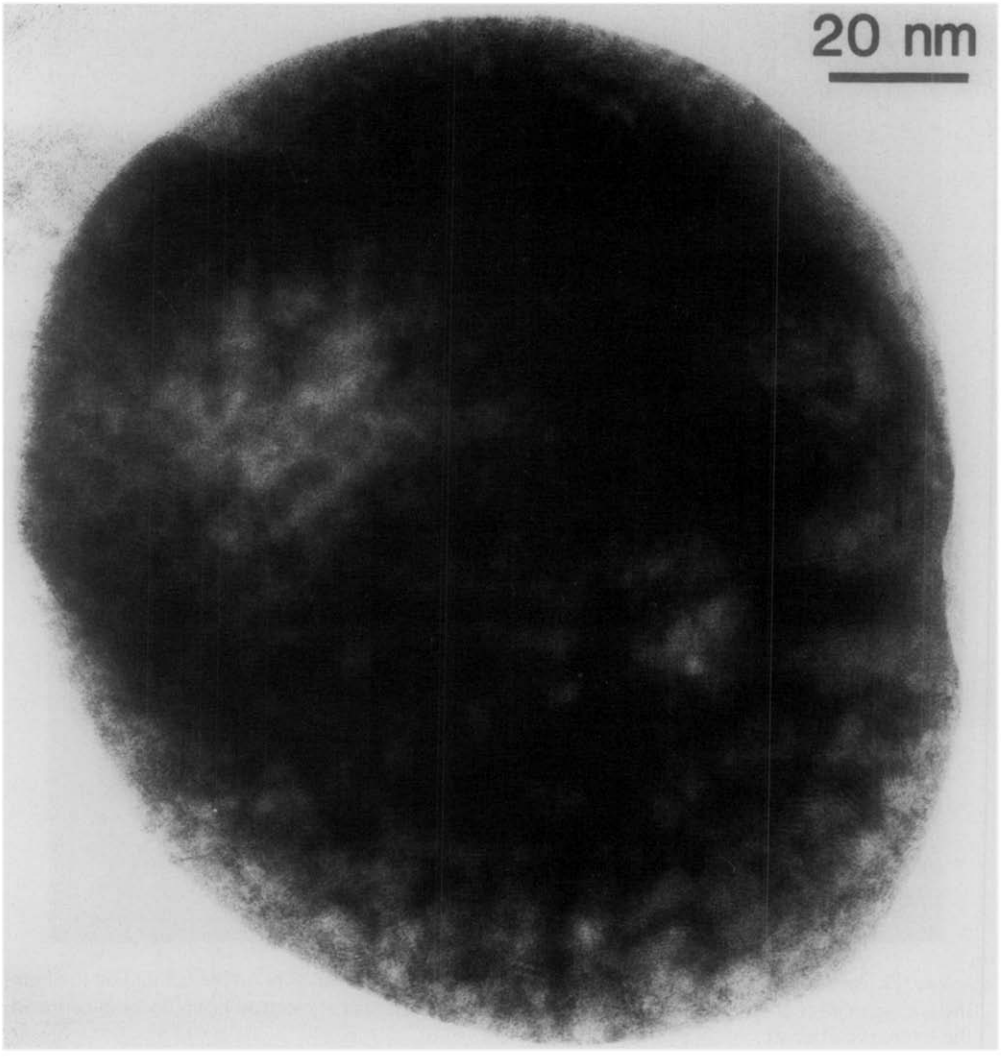

FIG. 12. A high-magnification image showing the effect of electron beam irradiation.

sponding more closely to that of $Tb(OH)_3$ as suggested by the streaked diffraction pattern placed above the top edge.

The model suggested from Fig. 15b is that the colloidal sphere, when it is precipitated, consists of a disordered network of small clusters of Tb atoms more or less cubicly coordinated by O or OH, and weakly cross-linked yielding space for water molecules and for local charge neutralization by CO_3^{-2} ions. As the particle ages in the vacuum of the microscope carbon dioxide and water diffuse outward and are lost from the surface regions first with concurrent nucleation of either oxide or hydroxide. These crystalline nuclei, scattered over the surface, grow to impingement and inward with time. The image of the surface confirms the growth of nuclei with orientations that lead to polygonization at later stages. It is clear

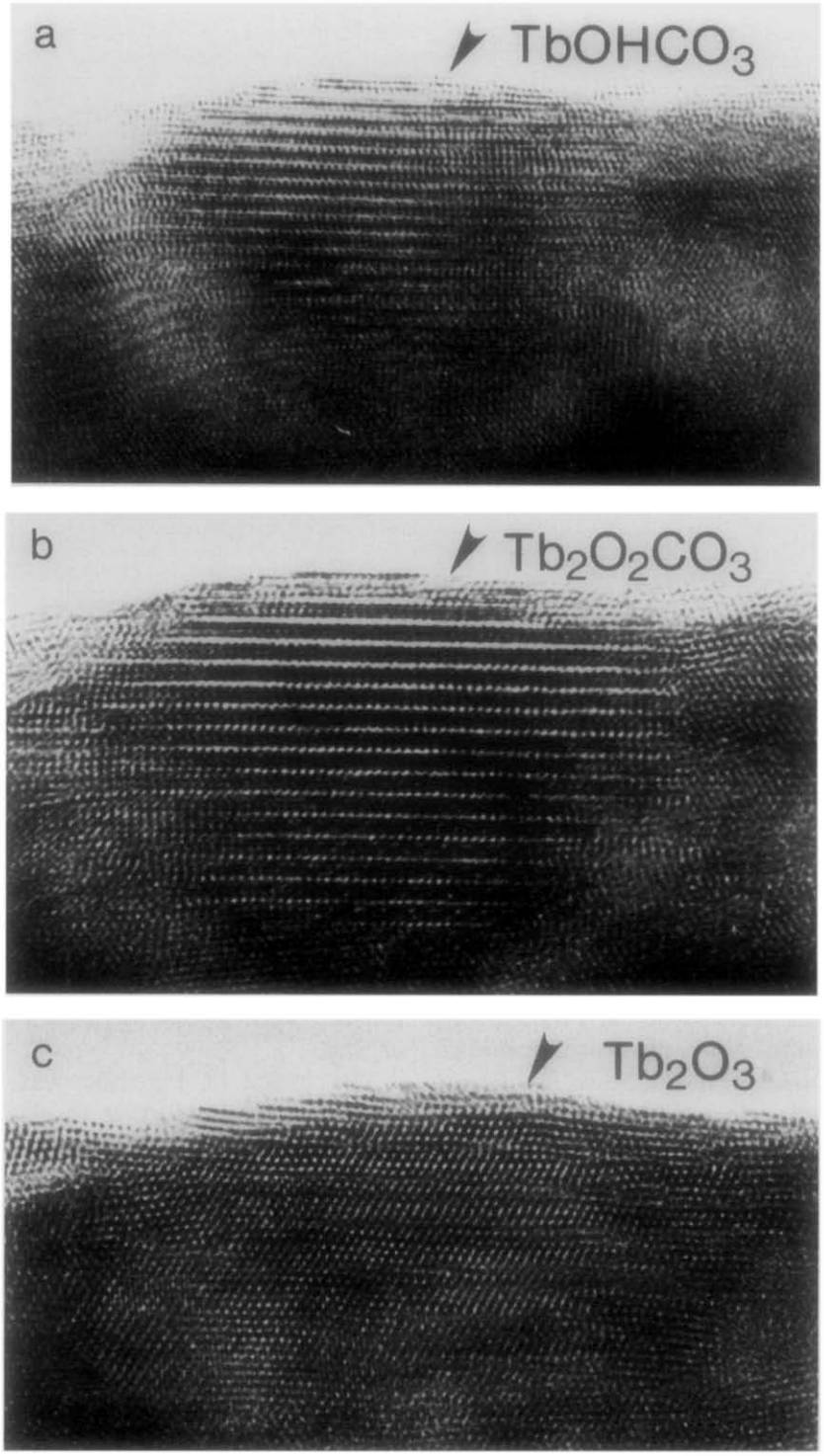

FIG. 13. High-resolution electron microscope images of the same region of the surface of the sphere shown in Fig. 12 after intervals of irradiation. At the top center is the hydroxycarbonate which transforms to the dioxymonocarbonate, then finally to mostly the sesquioxide.

FIG. 14. A small section of a precipitate having snowflake morphology is seen in this high-magnification image to consist of sintered polycrystalline spheres.

that the surface plays a dominate role in nuclear orientation. This phenomenon was also clearly demonstrated in an earlier report of the decomposition of neodymium hydroxycarbonate (*9*).

Figure 15c, of the same region of the particle, shows the cumulative change after 5 min of irradiation. Note particularly the growing polygonization of the surface profile, the orientational misfit of the grains resulting from the preferred surface nucleation, and the uneven inward growth of the crystalline surface layers. This unevenness of inward growth must arise from orientations more or less favorably placed to facilitate the loss of CO_2 and H_2O from the surface. Besides this crust, the interior of the sphere is vastly more ordered than before. Particular attention is directed to a region that is an intergrown overlay of the decomposition product, Type II $(TbO)_2CO_3$ in the [010] zone ($c \simeq 1.6$ nm), formed from water uptake.

The further development of the structures revealed in Fig. 15c are apparent in Fig. 15d taken 20 min later, but nowhere is it more apparent than in the region where $(TbO)_2CO_3$ previously existed. The new pattern can be identified as that of Type II $(TbO)_2CO_3$ in the $[1\bar{1}0]$ zone. This emphasizes the rapid transformations that occur as water and CO_2 are diffusing through the crystal.

The image in Fig. 15e was recorded 30 min later and further displays the remarkable mobility of this material. The same volume of the particle that became the decomposition product has now reversed the reaction and taken up CO_2 and H_2O and reverted to the original hydroxymonocarbonate. Eventually an imperfectly crystallized oxide occupied this region.

Conclusions

The sensitivity of the nanostructure of a colloidal gel and its mode of decomposi-

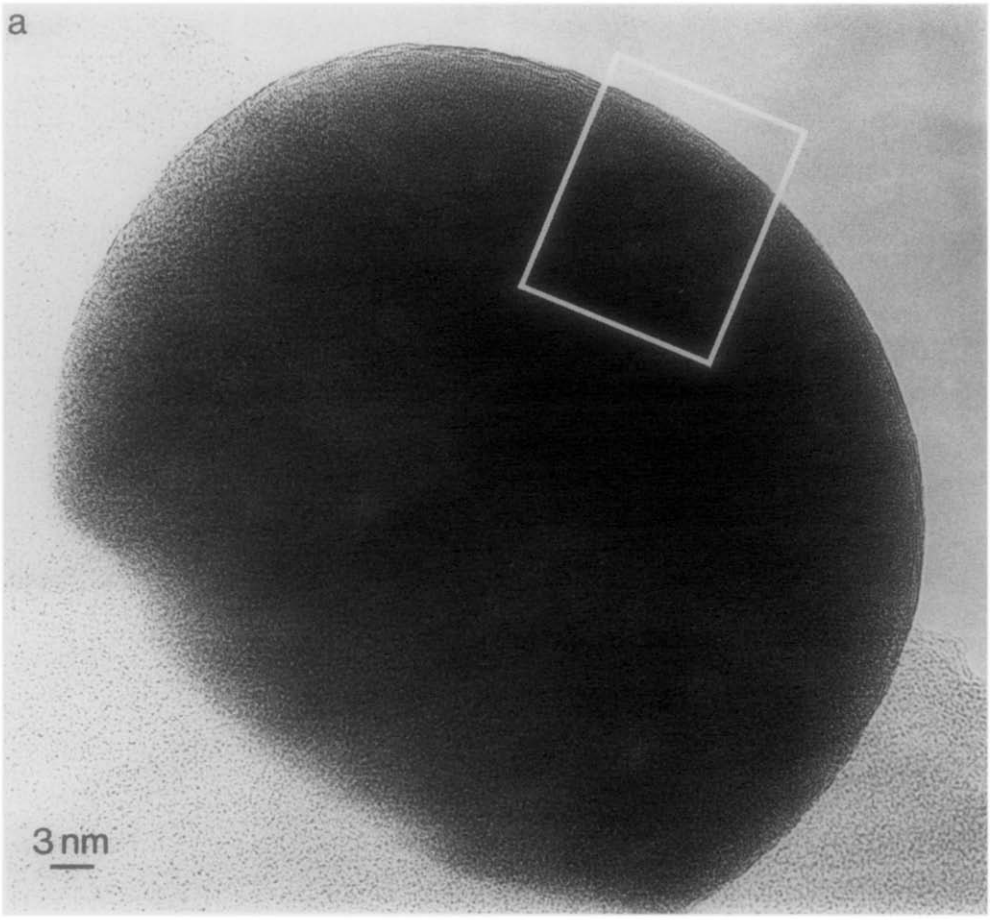

FIG. 15. (a) A high-resolution image of the 50-nm colloidal sphere to be subject to decomposition as documented in the subsequent figures. The region of study is marked. (b) A high-resolution image of a section of the 50-nm sphere showing significant short-range order even in the freshly prepared crystal. (c) The same region of the sphere as in (a) showing the great increase in order including a region of the Type II $(TbO)_2CO_3$. (d) An image showing an orientational transformation of the $(TbO)_2CO_3$. (e) An image showing the region having transformed primarily to $TbOHCO_3$.

tion in the electron beam is clearly demonstrated in these experiments. In the cerium and terbium materials the colloids were both prepared in two different ways and the lower temperature conditions produced spherical particles while the snowflake-like morphologies were formed at higher temperatures. In Ce(IV) materials, the product was mostly the dioxide with a small impurity, probably a complex sulfate. The decomposition of the terbium material was more complicated since it forms several intermediate compounds before the final oxide. The conditions used in the microscope were not harsh enough to produce the pure oxide from either morphology of the complex terbium carbonates.

The ceric material maintained a relatively compact form during decomposition whereas the terbium hydroxycarbonate suf-

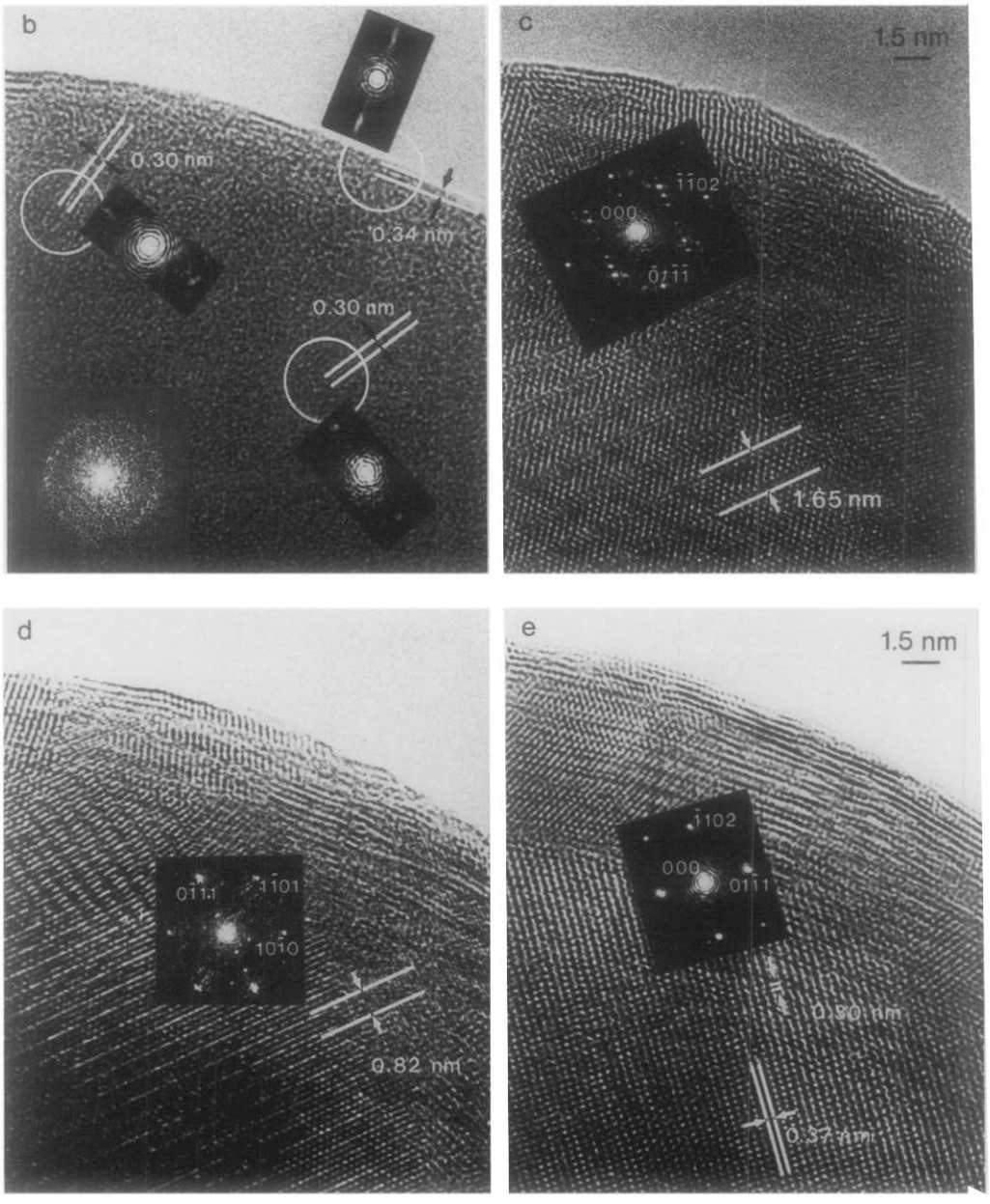

FIG. 15—*Continued*

fered the formation of large voids when intensely irradiated. This obviously relates to the liberation of carbon dioxide as well as water in the latter.

Neither material was amorphous at first but showed at least short-range order, even when produced under the mildest conditions. The gel spheres in both the

cerium and terbium colloids apparently consist of clusters where the metal atoms are in an essentially cubic close-packed arrangement. This is suggested by the broad diffuse bands of the optical diffraction patterns taken from the first images of the colloidal spheres. This suggests that such clusters exist in the solution and are crosslinked to form the colloid, locally incorporating neutralizing carbonate ions and water in the process. At a later stage these broad bands become sharper as fluorite-like ordered regions grow in the cerium colloids and as the intermediate compounds form in the terbium system.

The early stages of decomposition of the terbium hydroxycarbonate demonstrate a material capable of rapid chemical reaction as regions are swept by streams of diffusing carbon dioxide and water. At the surface edge the compounds apparently are limited to disordered oxides and hydroxides of variable composition because of the ready loss of the gaseous decomposition products to the vacuum of the microscope. In the interior, rapid crystallization of complex compounds respond quickly to changing local composition. Besides the general suggestion of initial fluorite-like clusters it is also important to notice that the spherical colloids sinter readily to give undefined boundaries and larger grains while the polycrystalline precipitates more or less maintain the grain boundaries as they perfect their crystallinity during aging.

Finally, the orientation of the polycrystalline specimens such as to be aligned along a principle axis during reaction is remarkable and suggests a direct electron beam effect on this labile system.

Acknowledgments

It is a pleasure to acknowledge the support of the NSF through Research Grant DMR-8820017 and the partial support of the Facility for High-Resolution Electron Microscopy through DMR-8611609.

References

1. D. R. Ulrich, "Chemical Processing of Ceramics," Chem. & Eng. News, January 1, p. 28 (1990).
2. J. J. Zelinski and D. R. Uhlmann, *J. Phys. Chem. Solids* **45,** 1069 (1984).
3. E. A. Barringer and H. K. Bowen, *J. Amer. Ceram. Soc.* **65,** C199 (1982).
4. J. Livage, M. Henry, and C. Sanchez, *Prog. Solid State Chem.* **18,** 259 (1988).
5. E. Matijević, *Annu. Rev. Mater. Sci.* **15,** 483 (1985).
6. W. P. Hsu, L. Rönnquist, and E. Matijević, *Langmuir* **4,** 31 (1988).
7. E. Matijević and W. P. Hsu, *J. Colloid Interface Sci.* **118,** 506 (1987).
8. J. R. Fryer, J. L. Hutchison, and R. Paterson, *J. Colloid Interface Sci.* **34,** 238 (1970).
9. H. Hinode, R. Sharma, and L. Eyring, *J. Solid State Chem.* **84,** 102 (1990).
10. H. Hinode, R. Sharma, and L. Eyring, to be published.
11. C. K. Jørgensen, "Inorganic Complexes, "Academic Press, London (1963).
12. J. Sawyer, P. Caro, and L. Eyring, *Rev. Chim. Min.* **10,** 93 (1973).